Polymerized carbon nitride nanobells

G. Y. Zhang, X. C. Ma, D. Y. Zhong, and E. G. Wang[a)]
State Key Laboratory for Surface Physics and International Center for Quantum Structures, Institute of Physics, Chinese Academy of Sciences, Beijing 100080, People's Republic of China

(Received 12 November 2001; accepted for publication 8 March 2002)

Well-aligned carbon nitride nanotubes are fabricated by microwave plasma assisted chemical vapor deposition using iron as the catalyst. These nanotubes are linearly polymerized by carbon nitride nanobells with catalyst particles in the root, as revealed by high-resolution transmission electron microscopy. Carbon nitride nanotube film is analyzed by x-ray photoelectron spectroscopy (XPS), Auger electron spectroscopy (AES), and Raman spectroscopy. Both XPS and AES reveal a nitrogen content of about 2% in the film. Raman spectroscopy exhibits a good crystallization of these carbon nitride nanotubes. Electron energy loss spectroscopy is used to study the local distribution of nitrogen in a single nanotube, which indicates that nitrogen prefers to locate at curved graphite sheets, at the top of the nanobells, and that incorporation of nitrogen results in the decrease of the crystallization. Based on these results, a growth model is proposed to explain this periodically stacked nanobell structure. In this model, we propose that graphite sheets only precipitate along the surface of catalyst particles and that lower growth rate at the top curve surface of the bell-like catalyst particle is the key factor influencing formation of this special microstructure. A heterojunction between a tubular carbon nanotube and a carbon nitride nanobell also has been fabricated by a two-step growth technique. And short carbon nitride nanotubes with a few nanobells or even just one nanobell are obtained by both physical and chemical methods. Furthermore, we studied the field emission properties and have obtained a threshold field of as low as about 1 V/μm. A novel side-emission mechanism has been proposed based on the special polymerized nanobell structures. © *2002 American Institute of Physics.* [DOI: 10.1063/1.1476070]

I. INTRODUCTION

Since the discovery of nanotube structures,[1] pure carbon nanotubes and related compound nanotubes (or nanofibers) built up by light elements, such as C–N, B–N, and B–C–N, have attracted much attention due to their novel electronic structures and mechanic properties, which are crucial for nano-device manufacturing. In the case of carbon nitride nanotubes (CNNTs), earlier theoretical calculations[2] demonstrated that semiconducting carbon nanotubes could be *n*-type doped by substitution of N atoms. Miyamoto *et al.*[3] investigated two kinds of possible tubule forms of carbon nitride. They estimated that the strain energies are lower to roll the C_3N_4 and CN graphite sheets into tubule forms, and they found that C_3N_4 tubules are insulating while CN tubules are metallic independent of tubule diameter and chirality.

Compared to the relatively few theoretical calculations, many experiments have been carried out. CNNTs are mostly synthesized by chemical vapor deposition (CVD) methods from precursor compounds containing two component elements, C and N. There are also reports on the arc-discharge method[4] and the dc magnetron sputtering method[5] used to synthesize CNNTs. The CVD methods have some advantages for growing CNNTs compared to the arc-discharge and laser ablation methods, such as lower growth temperature and easier control of growth conditions. Some CVD methods are reported, such as (a) thermal chemical vapor deposition (TCVD),[6–10] (b) microwave plasma enhanced/assisted chemical vapor deposition (MPCVD),[11–13] and (c) electron cyclotron resonance chemical vapor deposition (ECRCVD).[14,15] The N/C ratio of CNNTs is different in these studies. The highest N/C ratio reported is up to 0.72, but these nanotubes are totally amorphous.[14,15] Almost all CNNTs synthesized by methods (a) or (b) using iron as the catalyst showed periodic structures, usually called ''bamboo-like'' structures, instead of tubular forms. Similar structures can also be found when using cobalt or nickel as the catalyst. We obtained our CNNTs by using the MWCVD method.[11] Our results show that each CNNT has a linearly polymerized structure by a series of stacking truncated graphite cones, called a nanobell.

Many efforts have been made in the syntheses, but there still remain some long-standing questions. For example, why can CNNTs grow into such a periodic structure? Some growth models were proposed to answer this question; however, no sufficient and systematic experimental evidence supports these assumptions. In these models no attention was paid to the role of nitrogen during the formation of this structure. In our experiments, we find that nitrogen is a crucial factor in the formation of this CN nanobell structure, and using this property we can grow heterojunctions between carbon nanotubes and CNNTs.

In the present article we will describe the substrate preparation and MWCVD growth of CNNTs in Sec. II. The microstructure and chemical properties are presented in Sec.

a)Author to whom correspondence should be addressed; electronic mail: egwang@aphy.iphy.ac.cn

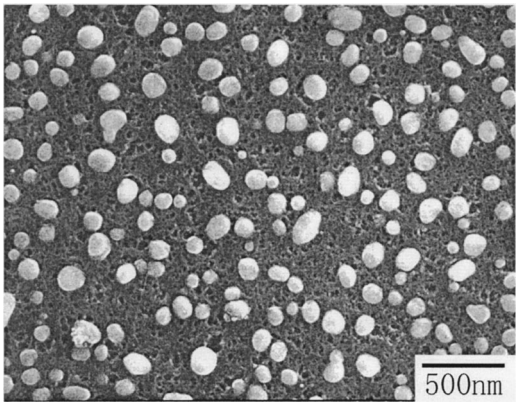

FIG. 1. SEM image of catalyst particles formed on Si substrate after pure N_2 plasma treatment for 2 min.

III. In Sec. IV we will discuss the growth mechanism in detail and explain some experimental results pertaining to the growth mechanism. We will also discuss the heterojunctions, short nanotubes, and their FEE properties in Secs. V–VII, respectively.

II. MICROWAVE PLASMA-ASSISTED CHEMICAL VAPOR DEPOSITION

In a previous letter[11] we described the use of mesoporous silica plates with nanometer-scale channels as substrates. Iron and nickel nanoparticles are filled into each channel of the mesoporous silica as catalysts. After the MWCVD process, CNNTs grow out from these channels. The diameter and orientation of the channel from which a CNNT grows mostly decides the diameter and orientation of that CNNT. In the present experiment, we use a Si wafer as the substrate on which a thin ferric oxide film is coated. CNNTs deposited on these substrates are highly aligned with uniform diameter.

The ferric oxide coatings are prepared by the sol-gel technique. We prepare $Fe(NO_3)_3$ sol and then drop the $Fe(NO_3)_3$ solution onto the rotating Si wafer. The coated samples are first air-dried at 100 °C for 15 min and then are heated at 500 °C for 30 min in an oxygen atmosphere to burn out organic material. After repeating the coating process several times we obtain a ferric oxide film of the necessary thickness.

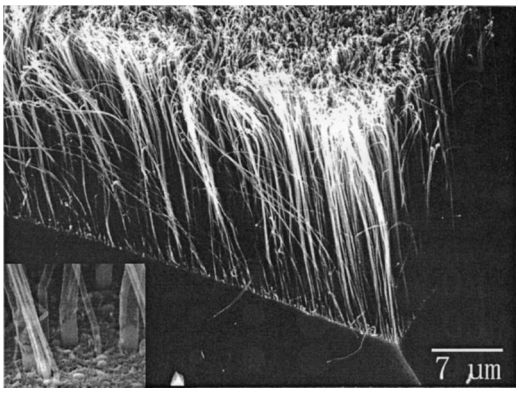

FIG. 2. SEM image of the well aligned CNNTs grown on Fe-coated Si substrate with an average length of 20 μm. The inset at the lower left shows the root of the CNNTs, which encapsulate catalyst particles.

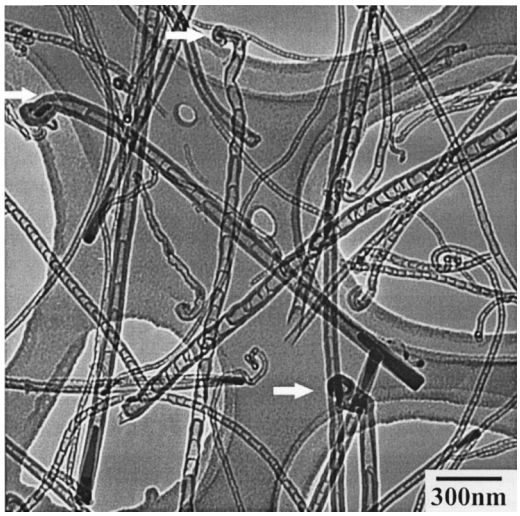

FIG. 3. TEM image of CNNTs exhibiting the polymerizing nanobells microstructure. Bell-like catalyst particles lay in the root of the CNNTs. Arrows denote the irregular shapes of tubes' ends.

The deposition system used in this study is a MWCVD system (ASTeX 2115) with a 2.45 GHz microwave power supply. The maximum microwave power is 1.5 kW. Microwaves enter the reaction chamber through a quartz entrance window and ignite the plasma on the substrate. The substrate can be heated up to 800 °C by a ratio-frequency heater independent of the ignited plasma. Only N_2 and CH_4 are introduced into the reaction chamber as gas feedstock.

Based on the experimental results we find that CNNTs can be obtained over a wide range of parameters: 450–800 °C substrate temperature, 150–1000 W microwave power, and 0.6–4.0 kPa growth pressure. The optimal growth conditions used in the present study are about 550 °C, 600 W, and 2.0 kPa. To decrease the etching of the plasma we usually put the substrate upside down and let the backside with no catalyst face the plasma. Before growth, a pure N_2 plasma treatment is needed to form catalyst particles and decrease the instability of the earlier growth. Figure 1 is a scanning electron microscopy (SEM) image of the catalyst particles after a 2-min treatment in pure N_2 plasma. The catalyst particles are not exactly equal in diameter (average ~100 nm) and do not generally have a regular sphere shape. After the formation of catalyst particles, methane (CH_4) is gradually introduced into the reaction chamber without shutting off the N_2 plasma. Figure 2 shows the image of the well-aligned, uniformly distributed CNNTs after a 30-min growth period. These tubes are grown using nitrogen and methane ($N_2/CH_4=50/1$) at a substrate temperature of 550 °C, microwave power of 600 W, and under pressure of 2.0 kPa. The average length of the CNNTs is about 20 μm. The diameter of the tubes range from ~20 to ~150 nm and the average diameter is about 80 nm. By observation of the CNNT roots we find that the catalyst particles are encapsulated in the root of the CNNTs, which indicates a base-growth mechanism (shown in the inset of Fig. 2). Most

tubes' tips are not straight; we conclude that this is caused by instability at the beginning of the growth period.

III. NANOBELL STRUCTURE

High-resolution transmission electron microscopy (HRTEM), electron energy loss spectroscopy (EELS), x-ray photoelectron spectroscopy (XPS), Auger electron spectroscopy (AES), and Raman spectroscopy (RS) are used to analyze the samples.

The CNNTs, scraped from the substrate and then ultrasonicated in ethanol, cover the copper microgrid for TEM, HRTEM, and EELS analysis. Figure 3 is a typical transmission electron microscopy (TEM) image of the CNNTs. It reveals that each nanotube consists of many compartments one by one. Along the nanotubes we find bell-like catalyst particles encapsulated in the root. The shapes of the compartments in one tube match quite well with the catalyst particle, seemingly indicating that the catalyst particle has lain in these compartments. Occasionally, at the nanotubes' end there are also some iron particles. Unlike those catalyst particles in the root of the nanotubes, these particles are totally capsulated in the nanotubes and we believe that they do not act as growth catalysts.

Figure 4 is a typical HRTEM image of part of a CNNT containing a catalyst particle. In this figure we can see that truncated graphite cones stack to form a nanotube, and that in every cave or in some cones a hollow compartment is formed. These truncated graphite cones terminate at the outer surface of the tube with opened edges (marked by the arrow in Fig. 4). We call it a ''nanobell,'' referring to a series of adjacent graphite cones paralleling to each other between two compartments. So our nanotubes are linearly polymerized by nanobells. Each nanobell consists of a curved top and nearly straight sides, which are not parallel but tilt at an angle to the tube's axis. Usually, longer nanobells are not linked directly to each other and between the adjacent two nanobells there often exist some transitional layers of graphite sheets without closed ends at the top. A detailed discussion of the shape formation will be given in the following section. In the case of shorter nanobells, the microstructure exhibits some differences. For one thing, the graphite sheets forming the nanobell are totally curved without straight sides, and the nanobells are linked to each other directly without transitional graphite layers.

Concerning the crystallization, the three kinds of CNNTs observed are summarized as follows.

(a) Most of the CNNTs in our samples exhibit good crystallization, and graphite sheets can be clearly seen by HRTEM. There is no interlinking or intersection between neighboring graphite layers. The tubes are polymerized by perfect nanobells.

(b) A few CNNTs with poor crystallization can be found, and graphite sheets in these tubes are not integrated but are interlinked with neighboring graphite sheets. These tubes still show a nanobell shape.

(c) Amorphous tubes are also found, but these tubes are very rare in the samples. No graphite sheets are present in these tubes.

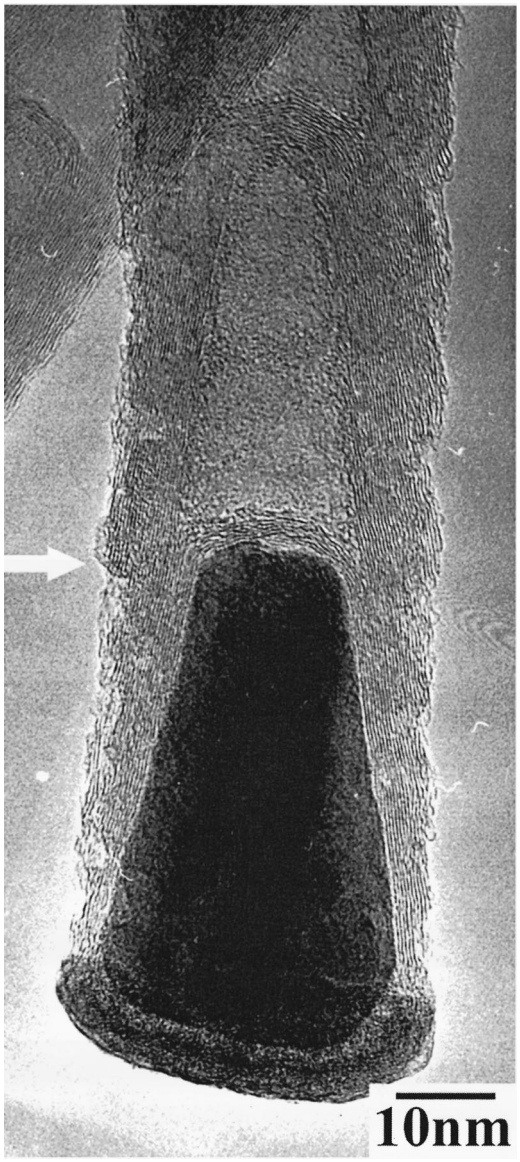

FIG. 4. HRTEM image of a typical CNNT containing a catalyst particle (dark region). Open edges of the nanobell (marked by the arrow) distribute on the outside surface. The lowest hook-shape region is assumed to be the Fe–C alloy, which is embedded in the polycrystalline film on the substrate, and from which carbon atom species are supplied then diffuse to the growth region during the growth. The damage on the outer surface is caused by the overlong ultrasonication in the sample preparation.

Combined with the HRTEM results, nitrogen in nanotubes is measured by EELS, XPS, and AES, and crystallization is analyzed by Raman spectroscopy.

A. EELS spectrum of CNNTs

The electron energy loss spectroscopy (EELS) is carried out by means of a field emission electron microscope JEM-2010 (JEOL) operating at 200 kV with a GIF system. EELS analysis of large quantities of CNNTs reveals that N content varies from one nanobell to another in a single CNNT, and also varies between different CNNTs. Even in one nanobell the N content varies between different regions. By comparing to the corresponding region where the N is detected, we can conclude that the N content is directly related to the microstructure of the nanobell. In a single nanobell the N

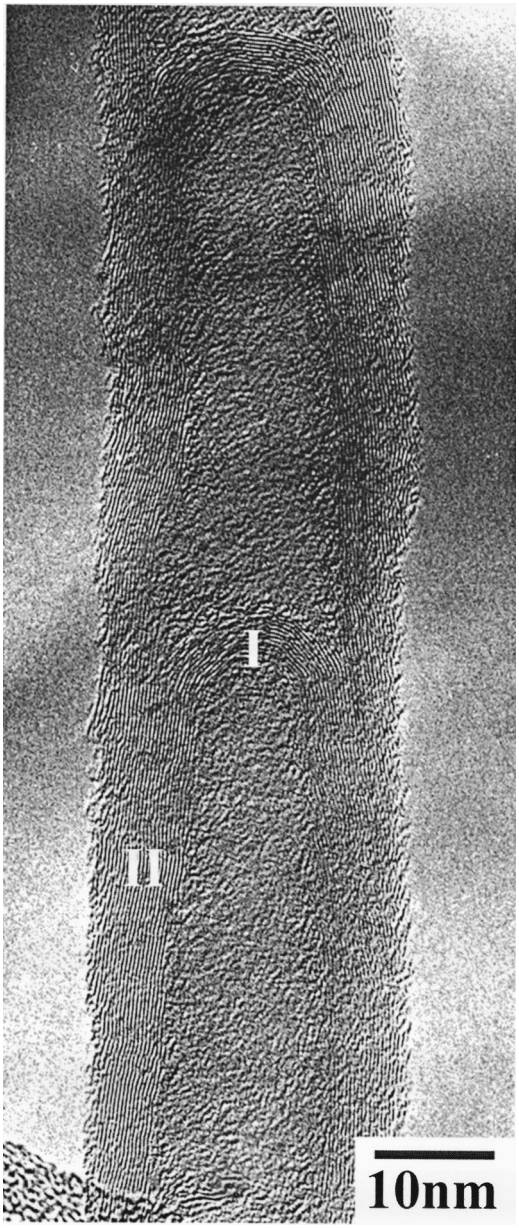

FIG. 5. HRTEM image of a well-crystallized nanotube.

content at the top with curved graphite sheets is higher than at the sides with straight graphite sheets. Figure 5 is a HRTEM image of a CNNT, and Figs. 6(a) and 6(b) show the typical EELS spectra at regions I and II marked in Fig. 5, respectively. Within region I a nitrogen content of ~6% is detected. But nitrogen content in region II is very low. Figure 6(a) shows ionization edges at ~284.5 eV corresponding to the characteristic *K* shell for carbon and at ~400 eV corresponding to the characteristic *K* shell for nitrogen. In Fig. 6(b) the peak located at ~400 eV is too weak to calculate the N content, but we are sure that the N content is less than 1%.

There also is a trend which seems to indicate that the poorer the crystallization, the higher the N content in the CNNTs. Usually, the average N content in a type II region is the highest and in a type I region is the lowest. The highest N content detected is 39%, and the HRTEM image shows us that the corresponding CNNT is completely amorphous.

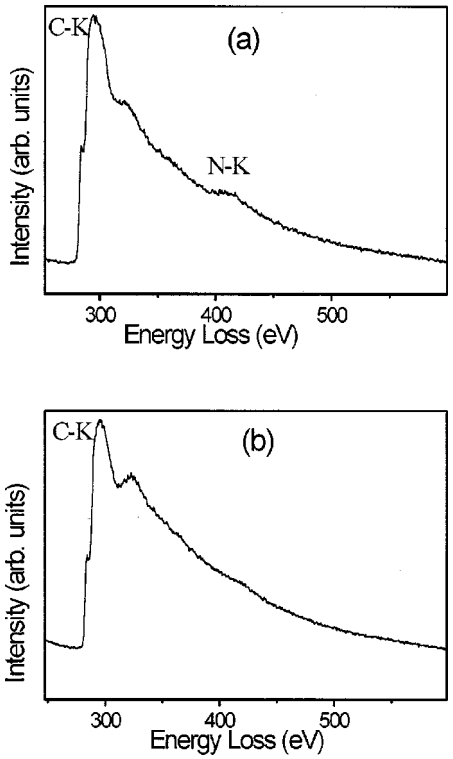

FIG. 6. (a) and (b) are EELS spectra corresponding to the I and II regions marked in Fig. 5, respectively. (a) exhibits *K*-shell ionization edges for C(~284.5 eV) and N(~400 eV). The N edge is very weak in (b).

B. XPS and AES studies of CNNTs film

Figure 7(a) is x-ray photoelectron spectra of $10 \times 10\ \mathrm{mm}^2$ CNNTs film after employing an argon ions beam etching for 2 min to remote the absorptive nitrogen and oxy-

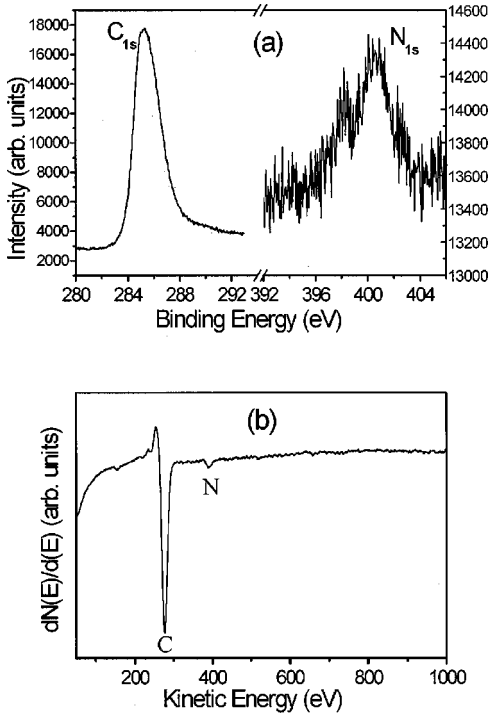

FIG. 7. (a) X-ray photoelectron spectrum and (b) Auger electron spectrum of the CNNTs thin film.

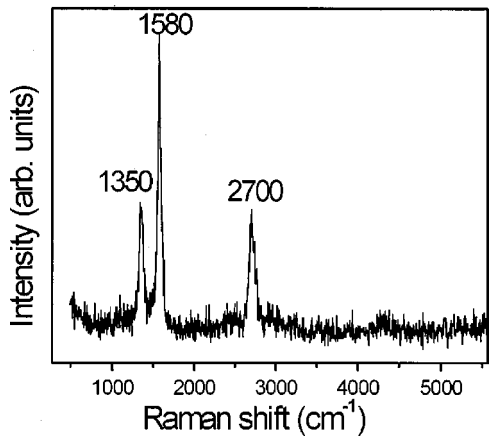

FIG. 8. Raman spectrum of the CNNTs thin film with 488.2 nm wavelength excitation.

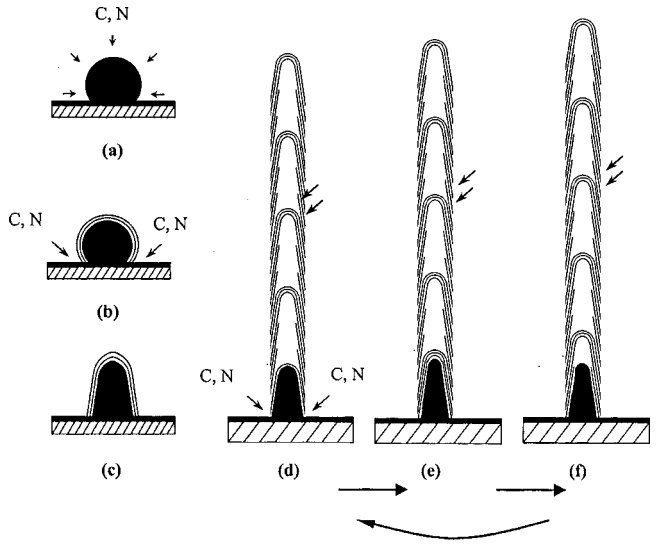

FIG. 9. Schematic figure of the growth process of carbon nitride nanobells. (a) Forming a quasispherical catalyst particle, (b) beginning to precipitate graphite sheets, (c) stretching the catalyst particle into a bell-like shape, (d) precipitating the first graphite layer of a nanobell when the top curvature of the catalyst is supersaturated with carbon, (e) stopping to growth at the top curvature of the catalyst particle, and (f) beginning to precipitate graphite sheets on the side surface of the catalyst particle.

gen. The sample was grown at a temperature of 550 °C and a microwave power of 550 W for a 30-min period with a gas flow rate of N_2/CH_4 (150/3). The pressure of the growth chamber was kept at 2.0 kPa during the growth. In Fig. 7(a) the C_{1s} peak is located at 285.4 eV, which corresponds to that of graphite. Two peaks of the N_{1s} are located at 398.8 and 401.0 eV, respectively. It is presumed that the former is characterized by a N atom just on the edge of the graphite layer, only bonded to two C atoms, while the latter corresponds to N atoms replacing C atoms in graphite layers and bonded to three C atoms.[16] In our case, because of the existence of open sides in the CNNTs (see Fig. 4), which introduce lots of graphite layer edges, the peak at 398.8 eV seems reasonable. By use of the ratio of the respective integrated peak areas and the photoionization cross-section rations for the 1*s* level, we find that the average nitrogen content of this specimen after argon ion sputtering is about 2 at. %. Due to the preferential etching of nitrogen in samples,[17] it is believed that the measured nitrogen content is lower than the actual one.

Auger electron spectroscopy (AES) analysis also gives the same results. Figure 7(b) is an AES spectrum of this sample after argon ion beam etching for 2 min. The N content shown in this spectrum is about 2 at. %, which is consistent with the XPS results.

C. RAMAN spectrum of CNNTs

Figure 8 shows a Raman spectrum of multiwalled CNNTs. First-order Raman spectrum shows a strong peak at about 1580 cm^{-1} (G mode), which is a characteristic of graphite sheets. Another strong peak at 1350 cm^{-1} is assigned as the disorder-induced D mode. The overtone of the D mode located at about 2700 cm^{-1} (2D) is observed, and this second-order Raman spectrum also shows a strong peak. A relatively weak peak at about 4280 cm^{-1} is also observed. This third-order Raman mode can be attributed to a combination of 2D+G mode.

The D-mode peak is attributed to a finite particle size effect or lattice distortion, such as defects in the curved graphite sheets, tube ends, or finite size crystalline domains in the nanotubes.[18] As described before, SEM and TEM analysis shows that our samples contain no carbonaceous particles, but unlike usual multiwalled carbon nanotubes, all CNNTs in our samples are polymerized by carbon nitride nanobells. Each nanobell consists of a series of curved graphite sheets, which is formed by introducing lattice distortion to the graphite layers. Additionally, we can deem a single nanobell a basic unit, and each nanobell plays a role in Raman scattering. So in our case, the strong D-mode peak can be due to three causes: (a) the finite size of the nanobells; (b) distortion in the curved graphite sheets; and (c) the high density of aligned nanotubes.

IV. GROWTH MODEL OF NANOBELLS

As mentioned above, in our experiments iron catalyst particles are encapsulated in the roots of nanotubes, which indicates a ''base-growth'' mechanism, and all CNNTs exhibit periodic bell-like structures. Here, based on the vapor-liquid-solid (VLS) growth mechanism,[19,20] we propose a discontinuous growth model to understand this nanobell microstructure.

This model consists of three steps: (a) formation of the catalyst particles on the substrate surface; (b) precipitation of the initial graphite sheets and stretching the quasi-spherical catalyst particles into bell shapes; and (c) and the growth of nanobells. The schematic pictures are given in Fig. 9, which can be described as follows.

A. Catalyst particles

It has long been known that the melting point of a nanoscale particle decreases with a decrease in size (called ''thermodynamic size-effect'').[21] A recent study has proposed that surface melting can be enhanced by curvature[22] and that at a given temperature, the thickness of the liquid layer is greater for a curved surface than for a flat one.[23] The substrate used

in our experiment is a silicon wafer precovered by a thin polycrystalline iron film. Before growth the substrate is heated to 550 °C by a rf power, and when pure N_2 plasma is ignited the temperature at the substrate surface can be drastically increased by the bombardment of positive ions and negative electrons (mainly ions). Under our experimental conditions we conclude that the temperature can reach about 900 °C at the surface of the film. At this temperature polycrystalline iron particles melt and incorporate into larger particles in order to lower the surface free energy. As shown before, Fig. 1 is an image of catalyst particles treated by pure N_2 plasma for 2 min. We find that the catalyst particles are nearly spherical.

B. Stretched bell-shape

After the catalyst particles are formed, methane is gradually introduced into the reactive chamber while other experimental parameters are kept unchanged. With the continual ionization of methane, active carbon particles dissolve into the bulk catalyst through the surface [see Fig. 9(a)]. At the same time active nitrogen particles also dissolve into the catalyst, a process which begins when the N_2 plasma is ignited, but the solubility of nitrogen in iron is lower than that of carbon. During growth, the nitrogen just acts as a doping element and the behavior of carbon is determinant. When the surface of the catalyst particles is supersaturated with carbon,[24] the first graphite sheet begins to precipitate on the surface of the catalyst particle, and once the graphite sheets cover the surface of the catalyst particle, carbon is supplied from the root of the catalyst particles [see Fig. 9(b)]. Due to its larger surface/volume ratio in nanometer scale, the diffusion coefficient and solubility of C or N in nanoparticles is larger than in the bulk materials, and this makes it possible to quickly and continuously precipitate graphite sheets.

Unlike the quasi-spherical shape of the catalyst particles before growth, from Fig. 3 we see that the catalyst particles all show truncated conical shapes or bell-like shapes. By comparing these particles with the shape of nanobells, we can conclude that this bell-like shape is not formed due to cooling after growth. The deformation indicates that catalyst particles must have undergone stretching from a quasi-spherical shape to a bell-like shape, and also indicates that catalyst particles are in liquid or quasi-liquid state during growth. The reason for this stretching is not clear. We conclude that wetting or interplay between the surface of the catalyst particle and the graphite sheets is one possible reason for this stretching; gravitation is another. Sometimes catalyst particles can even be stretched into two parts and the upper part stays in the tip of the nanotube during growth. This is why we can also find iron particles in the tube's end in some CNNTs (shown in Fig. 3). By SEM and TEM analysis we find that nearly all the ends of CNNTs are irregular and usually have a comparable length of one or two nanobells. This irregular shape of the first ''nanobell'' is probably formed because of the unsuitability of the initial growth. For simplicity's sake, this irregular ''nanobell'' is drawn into a regular one in Fig. 9(c). Once there forms a stable catalyst particle (often after the formation of the first nanobell), the growth of the nanobell is stable.

C. Polymerized nanobells

In our experiments we also used hydrogen instead of nitrogen as our feed gas, keeping the other experimental parameters unchanged. In this case, pure carbon nanotubes can be obtained, which show no difference from common coaxial nested tubules. Once the N_2 is introduced, however, the nanotubes change into nanobell structures. This indicates that without the introduction of N, graphite sheets will no longer precipitate at the top surface of the catalyst particles. XPS, AES, and EELS spectra all exhibit the existence of N doping into graphite sheets at the top. Especially, EELS results show that the N prefers to exist in regions of curvature.

It is known that the introduction of pentagons can cause the curvature of a planar graphite layer. A theoretical calculation points out that N atoms incorporated during growth prefer a nonplanar surrounding, as in the curved structure around a pentagon, and pentagons become more stable than in the absence of N atoms.[25] In our experiment, due to the existence of large amounts of nitrogen atoms in the catalyst, curved graphite sheets with many pentagon rings are easier to form over the top surface of the catalyst, reducing the total energy of the formation.

But why do nanobells exhibit a periodic structure in one tube? Zhang *et al.*[26] suggest that the periodic sucking of the liquid catalyst particle into the nanobell causes this structure. In our case, this theory is not suitable. If this was what happened, the lengths of the catalyst particles would be distributed randomly once growth stopped. So we would find different shapes of catalyst particles by TEM analysis. In fact, the shapes of catalyst particles are similar, although they differ in size. Furthermore, in our samples the catalyst particles are completely encapsulated in the nanotubes and the shapes of the nanobells are similar to the catalyst particles, so it is difficult to imagine that it could be possible to allow the catalyst particles to change form to such an extent.

In our experiments, if the precipitation at the top of catalyst particle was continuous (which would mean the whole growth process was continuous), then the bell-like graphite sheets would be continuous or quasi-continuous along the axial of the tube. But we do not find this kind of CNNTs based on the experimental results. From the HRTEM image of the nanobells (shown in Fig. 4) we can see some conical graphite sheets without closed caps and having open edges at both the outside and the inside surface between two nanobells [shown in Figs. 9(d)–9(f) by the upper two arrows]. This directly suggests that the precipitation of the graphite sheets on the top surface is not continuous, but rather that it stops periodically.

One key point here is that the graphite sheets precipitate only along the surface of the catalyst. Active carbon particles are supplied from the bottom margin of the catalyst (see Fig. 9) and diffuse through the bulk catalyst to the surface where the graphite sheets precipitate. For simplicity's sake, we assume that it is an equilibrium state (or a supersaturating state) at the side surface of the catalyst, that is, within a fixed

time interval quantities of carbon atoms diffusing from the root of the catalyst are equal to those precipitating at the side surface. However, at the top of the surface this supersaturating state cannot be maintained. Due to the relatively great diffusion distance, supplements of carbon atoms at the top surface will be slower than those at the side surface when precipitating the same layers of graphite sheets within the same time interval. So carbon content at the top surface decreases gradually, with carbon atoms continuously precipitating. We conclude that when the supersaturating state is damaged, the precipitation of graphite sheets does not cease immediately, due to the interplay between the graphite sheet and the catalyst surface. For example, precipitation of graphite sheets is endothermic and cools the catalyst particle.[19] The cooling stimulates further precipitation of the graphite sheet as a result of the reduction of the carbon's solubility. Once the precipitation on the top surface is stopped, it will not resume precipitation until the catalyst particle on the top of the surface supersaturates once again. But on the side surface precipitation continues and cone-shaped graphite sheets without closed caps are formed. Figures 9(d)–9(f) demonstrate the schematic process of the growth of a single nanobell.

Another notable phenomenon is that the curvature of the graphite sheet in a single nanobell decreases with coordinate increasing along the tube axial. We can imagine that if the catalyst particle did not change shape during growth, all graphite sheets would be the same and could not be stacked one after another. During a single nanobell's growth, when precipitating a new graphite sheet, the catalyst particle can be elongated due to space limitations created by previously formed nanobells. This elongation cannot stop until the precipitation suspends on the top surface. Once this suspension happens on the top surface, carbon atoms supplied from the root gradually regain a supersaturated state at the same time as the catalyst particles begin to recover to their original shape. The formed nanobell would be pushed up further with the recovering of shape due to the horizontal enlargement of the catalyst. Graphite sheets only precipitate on the side surface of the catalyst without closed caps. So a hollow compartment is formed. When the supersaturated state at the top surface is recovered a new nanobell begins to form. The above course repeats periodically and thus forms the polymerized nanobell structure.

V. HETEROJUNCTION

Heterojunctions between dissimilar nanotubes are essential in nanoscale electronic devices. There are some reports on the subject of fabricating the heterojunctions of carbon nanotubes/B–C–N nanotubes,[27] MWCNTs (multiwalled carbon nanotubes)/Si nanowires,[28] and SWCNTs (single-walled carbon nanotubes)/carbide nanorods.[29] But the relatively complex fabricating courses[23,24] and uncontrollability of the heterojunction growth processes make application less practical.

Since the growth of a carbon nitride nanobell strongly depends on the induction of N atoms as mentioned above, we can easily control the growth mode between carbon nitride and carbon nanotubes. By the use of CH_4 and H_2 (or N_2) as gas feedstock, we can grow pure carbon nanotubes or carbon nitride nanobells. We can also fully control the fabrication of C–N/C [see Fig. 10(a)] or C/C–N [see Fig. 10(b)] heterojunctions by changing the order of gas feedstock introduction during growth.

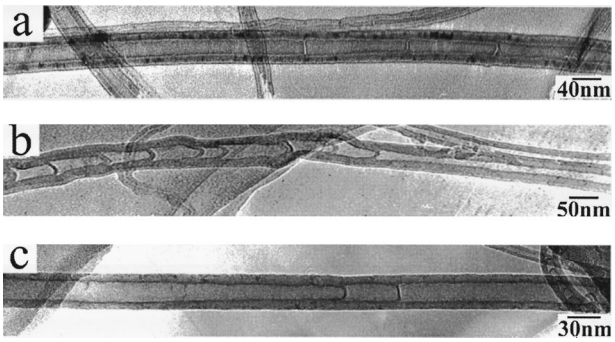

FIG. 10. TEM images of heterojunctions between a CNNT and a pure carbon nanotube. (a) Heterojunction of CNNT/CNT, (b) heterojunction of CNT/CNNT, and (c) biheterojunction of CNT/CNNT/CNT.

In order to obtain C/C–N heterojunctions we first grew carbon nanotubes with H_2 and CH_4 ($H_2/CH_4=1/1$) for 10 min, then grew C–N nanotubes by shutting off the H_2 and at the same time introducing N_2 instead ($N_2/CH_4=5/1$) for 10 min. The whole process maintains constant pressure. Figure 10(b) shows a transition electron microscopic (TEM) image of this kind of heterojunction. From it we can see that the upside is the cylindrical carbon nanotube and the downside is the C–N nanobells.

C–N/C heterojunctions are grown by a reverse process,[13] and the TEM image is shown in Fig. 10(a). From it we can see that the carbon nanotube is a nested coaxial tubule and the C–N nanotube is the polymerized nanobells.

We can also fabricate a biheterojunction of C/CN/C based on the same growth mechanism. For example, we first grew pure carbon nanotubes, then introduced a little N_2 to grow nanobells, and finally grew pure carbon nanotubes again. The resultant biheterojunction is shown in Fig. 10(c).

VI. SINGLE NANOBELL AND SHORT NANOTUBES

The study of short nanotubes has attracted much attention recently because of the requirements for continuously reduced device size and potential applications in the chemical industry. Previous studies show two ways to get short nanotubes: one is to control the growth time and another is to cut a long nanotube into short pieces. However, both methods are less than desirable due to their low productivity and the difficulty of employing them. Based on the special structure of the CNNTs here we have developed a new method to easily separate long nanotubes into short ones.

As discussed above, the basic unit of the CNNTs is the nanobell, which connect with each other by van der Waals bonds. Therefore the connection between adjacent nanobells is relatively weak and we can separate them by either physical or chemical methods.[12]

In this study, CNNTs are scraped from the Si substrate and then ground in a mortar with a few drops of ethanol for

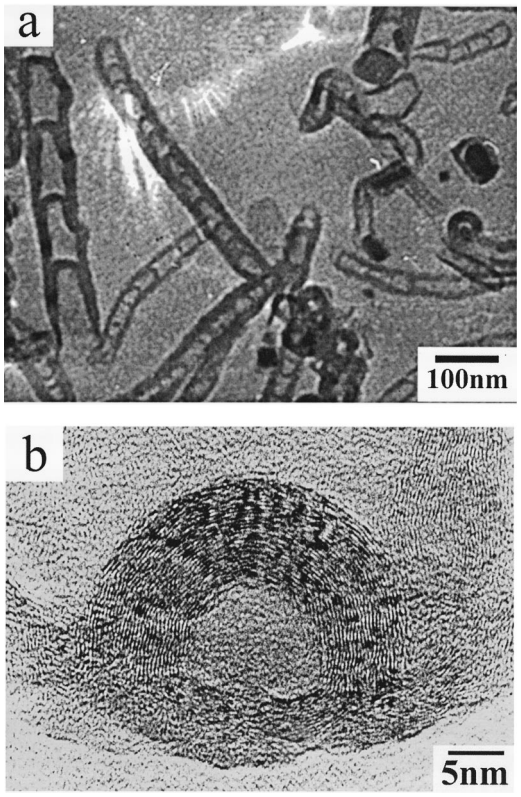

FIG. 11. (a) TEM image of short CNNTs obtained by a physical method. (b) A single nanobell obtained by a chemical method.

10 min. The obtained black powder is analyzed by TEM, and many short nanotubes with several nanobells can be observed in Fig. 11(a). A single nanobell can also be obtained by this chemical method. We first place long CNNTs into diluted sulfuric acid and disperse by sonication for 30 min, then add potassium permanganate and heat at 60 °C. Because the reaction rate is hard to control, we extract a part of the solution and neutralize with sodium hydroxide at varying time intervals. Finally we observe a perfect single nanobell, shown in Fig. 11(b).

VII. FIELD-EMISSION PROPERTIES

The field-emission tests are performed at room temperature in a vacuum chamber at a base pressure of $\sim 10^{-8}-10^{-9}$ Torr using a molybdenum anode with a tip diameter of ~0.1 mm. The distance between the sample ($7 \times 7\ \mathrm{mm}^2$) surface and the anode can be controlled with a precision level of 10 μm. The electrical field can be controlled by adjusting the space between the anode and the cathode, or by varying the applied voltage. In this experiment, a fixed gap distance of 0.7 mm is used. No field-emission current is observed when the applied electric fields are lower than about 1 V/μm. Figure 12 is a typical $I-V$ curve for field emission, where a Fowler–Nordheim plot is inserted. The plot is no longer heading in the former direction when the field increases to above ~2 V/μm. No current saturation is found under a high electric field. We conclude that such an excellent field emission results for the following reasons. First of all, the catalyst particles lie in the bottom of the nanotubes as shown above. Electrons are more difficult

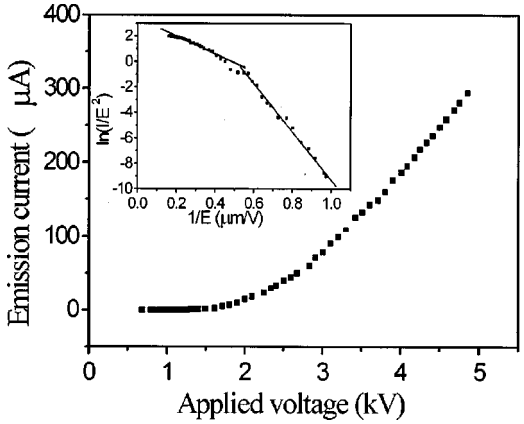

FIG. 12. $I-V$ characteristic of the CNNTs' film with an anode-sample distance of 600 μm. The inset is the Fowler–Nordheim plot.

to emit from metal than carbon nanotubes. That the catalyst lay on the top of the nanotubes will reduce the emission property. Another reason is that the work function of CNNTs in our sample (about 4.3 eV measured by ultraviolet photoelectron spectroscopy) is about 0.4 eV, which is smaller than that of the carbon nanotubes. Most import of all, in our samples the CNNTs are polymerized by nanobells, and on the outside surface of the CNNTs there exist many opened graphite sheets. We conclude that it is just because of the existence of the circular open edges that the emission can be enhanced under a high electrical field. That means that electrons can emit not only from the tops of the nanotubes but also from the side surfaces, which contributes to the increased high emission current density of field emission. Further *ab initio* calculations show that the electronic density of states at the open edges is very high.[30]

VIII. SUMMARY

In summary, we have shown that MPCVD is an efficient method of growing aligned CNNTs with a polymerized nanobell structure on a Si substrate precoated by iron catalyst. The most prominent advantage of this method is the controllable growth of the CNNTs, which makes it practical to grow heterojunctions between CNNT and CNT. By studying the spatial distribution of N in a single nanobell, we find that N atoms prefer to exist in locations with curvature, that is, in the curved nanobell's tip. The nanobells with better crystallization each contain a small amount of N; however, nitrogen content in some nanotubes with poorer crystallization can be very high. The average nitrogen content in the CNNT samples is 2%, as detected by XPS and AES. Raman spectroscopy has been used to study the crystallization of CNNTs, and HRTEM was used to study the details of the structures. Based on the bottom-growth mechanism we propose a discontinuous growth model to explain the formation of nanobells.

The main point of this model has the following two aspects. One is that graphite sheets only precipitate on the whole surface of the catalyst particle as a replica of the previous one. The other is the periodic supersaturation of C at the tip of the catalyst particle due to the long diffusion length

of carbon atoms, which results in the discontinuous growth of nanobells. We have also developed an easy method of obtaining short nanotubes with several nanobells by post-treatment of the CNNTs. Furthermore, a good FEE property with high emission current is observed from the polymerized nanobell structures, which shows the potential for flat panel display application. A side-emission mechanism based on the bell structures is proposed to explain the excellent emission property.

ACKNOWLEDGMENTS

The authors acknowledge the financial support of the NSF of China and the National Key Project for Basic Research (G2000067103). The authors also thank S. B. Zhang (RENL) for many helpful discussions.

[1] S. Iijima, Nature (London) **354**, 52 (1991).
[2] J.-Y. Yi and J. Bernhole, Phys. Rev. B **47**, 1708 (1993).
[3] Y. Miyamoto, M. L. Cohen, and S. G. Louie, Solid State Commun. **102**, 605 (1997).
[4] O. Stephan, P. M. Ajayan, C. Colliex, Ph. Redlich, J. M. Lambert, P. Bernier, and P. Lefin, Science **266**, 1683 (1994).
[5] K. Suenaga, M. P. Johansson, N. Hellgren, E. Broitman, L. R. Wallenberg, C. Colliex, J.-E. Sundgren, and L. Hultman, Chem. Phys. Lett. **300**, 695 (1999).
[6] M. Terrones, N. Grobert, J. Olivares, J. P. Zhang, H. Terrones, K. Kordatos, W. K. Hsu, J. P. Hare, P. D. Townsend, K. Prassides, A. K. Cheetham, H. W. Kroto, and D. R. M. Walton, Nature (London) **388**, 52 (1997).
[7] M. Terrones, H. Terrones, N. Grobert, W. K. Hsu, Y. Q. Zhu, J. P. Hare, H. W. Kroto, D. R. M. Walton, Ph. Kohler-Redlich, M. Rühle, J. P. Zhang, and A. K. Cheetham, Appl. Phys. Lett. **75**, 3932 (1999).
[8] W. Q. Han, P. Kohler-Redlich, T. Seeger, F. Ernst, M. Rühle, N. Grobert, W. K. Hsu, B. H. Chang, Y. Q. Zhu, H. W. Kroto, M. Terrones, and H. Terrones, Appl. Phys. Lett. **77**, 1807 (2000).
[9] K. Suenaga, M. Yudasaka, C. Colliex, and S. Iijima, Chem. Phys. Lett. **316**, 365 (2000).
[10] R. Sen, B. C. Satishkumar, A. Govindaraj, K. R. Harikumar, M. K. Renganathan, and C. N. R. Rao, J. Mater. Chem. **7**, 2335 (1997).
[11] X. Ma, E. G. Wang, W. Z. Zhou, D. A. Jefferson, J. Chen, S. Z. Deng, N. S. Xu, and J. Yuan, Appl. Phys. Lett. **75**, 3105 (1999).
[12] X. Ma, E. G. Wang, R. K. Tilley, D. A. Jefferson, and W. Zhou, Appl. Phys. Lett. **77**, 4136 (2000).
[13] X. Ma and E. G. Wang, Appl. Phys. Lett. **78**, 978 (2001).
[14] S. L. Saung, S. H. Tsai, C. H. Tseng, F. K. Chiang, X. W. Liu, and H. C. Shih, Appl. Phys. Lett. **74**, 197 (1999).
[15] S. L. Sung, S. H. Tsai, X. W. Liu, and H. C. Shih, J. Mater. Res. **15**, 502 (2000).
[16] J. Casanovas, J. M. Ricart, J. Rubio, F. Illas, and J. M. Jimenz- Mateos, J. Am. Chem. Soc. **118**, 8071 (1996).
[17] C. Ronning, H. Feldermann, R. Merk, H. Hofsäss, P. Reinke, and J.-U. Thiele, Phys. Rev. B **58**, 2207 (1998).
[18] W. Z. Li, H. Zhang, C. Y. Zhang, Y. Zhang, L. W. Xu, K. Zhu, and S. S. Xie, Appl. Phys. Lett. **70**, 2684 (1997).
[19] R. T. Yang and J. P. Chen, J. Catal. **116**, 52 (1989).
[20] W. L. Holstein, J. Catal. **152**, 42 (1995).
[21] F. G. Shi, J. Mater. Res. **9**, 1307 (1994).
[22] R. Kofman, P. Cheyssac, A. Aouaj, Y. Lereah, G. Deutscher, T. Ben-david, J. M. Penisson, and A. Bourret, Surf. Sci. **303**, 231 (1994).
[23] R. Garrigos, P. Cheyssac, and R. Kofman, Z. Phys. D: At., Mol. Clusters **12**, 497 (1989).
[24] E. F. Kukovitsky, S. G. L'vov, and N. A. Sainov, Chem. Phys. Lett. **317**, 65 (2000).
[25] H. Sjöström, S. Stafström, M. Boman, and J.-E. Sundgren, Phys. Rev. Lett. **75**, 1336 (1995).
[26] X. X. Zhang, Z. O. Li, G. H. Wen, K. K. Fung, J. L. Chen, and Y. D. Li, Chem. Phys. Lett. **333**, 509 (2001).
[27] Y. Zhang, H. Gu, K. Suenaga, and S. Iijima, Chem. Phys. Lett. **279**, 264 (1997).
[28] J. Hu, M. Ouyang, P. Yang, and C. M. Lieber, Nature (London) **399**, 48 (1999).
[29] Y. Zhang, T. Ichihashi, E. Landree, F. Nihey, and S. Iijima, Science **285**, 1719 (1999).
[30] G. L. Zhao, D. Bagayoko, and E. G. Wang (unpublished).